17 (2025) 100491

Contents lists available at ScienceDirect

Carbon Capture Science & Technology

journal homepage: www.elsevier.com/locate/ccst

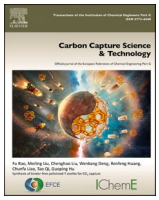

Full Length Article

Kinetic model describing the effect of amine loading and temperature on CO_2 capture by solid amine adsorbent

Shun Wang, Mengyin Xie, Shujuan Wang, Yuqun Zhuo *

Tsinghua University China

ARTICLE INFO

Keywords:
Solid amine adsorbents
kinetic model
CO_2 diffusion
carbon capture

ABSTRACT

The increasing CO_2 concentration in atmosphere leads to significant ecological changes, and the control of CO_2 emissions has been a major concern worldwide. Amine-functionalized adsorbents are promising because they have high CO_2 adsorption capacity, moderate adsorption heat and strong water resistance. Adsorption kinetics is a key performance parameter and facilitates the cognizance of microscopic CO_2 adsorption process. A novel kinetic model was proposed, which categorized the amines of solid amine adsorbents into two regions: the open amine region and the closed amine region. Different from the open amine region, CO_2 adsorption by amines in the closed amine region was significantly influenced by diffusion. The model could elucidate the effect of amine loading and temperature on CO_2 adsorption. When amine loading was below the theoretical maximum loading, the CO_2 adsorption capacity and the N efficiency gradually increased with the rise of amine loading. Nevertheless, as the amine loading further increased, the adsorption capacity decreased instead. CO_2 adsorption by solid amines was not affected by external diffusion, but was significantly affected by internal diffusion. The percentage of closed amine region of adsorbents with high amine loading was large, CO_2 needed to diffuse slowly into this region, leading to a small CO_2 adsorption capacity at low temperature. When the amine loading was less than 0.5, the CO_2 adsorption rate stayed almost the same. The model is instructive for the targeted preparation of solid amine adsorbents with fast adsorption rates.

1. Introduction

Carbon dioxide (CO_2) in atmosphere is the main anthropogenic greenhouse gas (Younas et al., 2020) and is responsible for climate change (Carlson et al., 2022; Daryayehsalameh et al., 2021; Szima et al., 2019). In 2023, about 37.4 Gt CO_2 was emitted to the atmosphere. Greatest Of all CO_2 sources, the power sector accounted for 36% of total emissions. Meanwhile, Coal remained the largest single source of electricity generation worldwide, and by far the largest CO_2 emission source of electricity sector: it contributed just over one-third of electricity generation but was responsible for nearly three-quarters of CO_2 emission in electricity sector (Birol, 2023; Dale, 2022). Therefore, decarbonization of power systems, especially coal-fired power plants, is of great importance for carbon reduction.

Due to the moderate binding energy with CO_2, amine is widely used for coal-fired flue gas carbon capture and direct air carbon capture (Chuah et al., 2025; Veluturla et al., 2025). However, amine itself is highly viscous and has low CO_2 diffusivity, thus showing a slow CO_2 adsorption rate(Tang et al., 2025). To improve its CO_2 diffusivity, two main approaches have been taken, one is amine solution (Meng et al., 2025; Zhang et al., 2024), which mixes amines with low-viscosity liquids such as water, and the other is solid amine adsorbents (Hu et al., 2025), where amines are loaded onto porous materials. Solid amine adsorbents have high adsorption capacities, selectivity and water resistance, and are regarded as one of the most prospective CO_2 capture agents (Sayari et al., 2011; Siegelman et al., 2021; Zhao et al., 2021).

Analyzing adsorption kinetics is important for reactor sizing and process optimization. Current studies on adsorbents mostly use simple adsorption rate models, such as pseudo-first-order model, pseudo-second-order model and Avrami kinetic models (Xu et al., 2024). Teng (Teng et al., 2024) found that the pseudo-second-order model could fit the adsorption experiment well, thus inferring that both chemical and physical adsorption occurred during the CO_2 uptake. Liu (Liu et al., 2014) utilized Avrami kinetic model to fit well the adsorption rate of TEPA carbon nanotube. He also proposed that the exponent n in the model mainly indicated the growth adsorption mechanism, and that the exponent did not vary with temperature, but varied with concentration. Serna (Serna-Guerrero and Sayari, 2010) used pseudo-first and Avrami

* Corresponding author.
E-mail address: zhuoyq@tsinghua.edu.cn (Y. Zhuo).

https://doi.org/10.1016/j.ccst.2025.100491
Received 12 June 2025; Received in revised form 18 August 2025; Accepted 19 August 2025
Available online 20 August 2025

kinetic models to fit the mass change curve measured by thermogravimetric analysis and applied the obtained adsorption rates to construct fixed bed column model. The models mentioned above could describe the total adsorption rate to some extent, which may be sufficient for engineering design, but are unable to describe the detailed CO_2 adsorption process and guide the preparation of solid amine adsorbents.

CO_2 adsorption by solid amine adsorbents involves several processes (Bos et al., 2019): external diffusion of ambient CO_2 into solid amine adsorbent particles; intraparticle diffusion inside the pores of adsorbent particle; CO_2 diffuses through the surface reacted amine layer to reach the deep unreacted amine region and then CO_2 react with amine. However, few studies on the adsorption kinetics of solid amine adsorbents provide a comprehensive discussion of the CO_2 adsorption process. Some studies determined whether the CO_2 adsorption process involves the above mass transfer resistance by collating the adsorption curve and Boyd's film-diffusion model, interparticle diffusion model, and intraparticle diffusion model (Yan et al., 2023; Yang et al., 2022). A poor fit to a model indicated that the adsorption process involved a corresponding mass transfer resistance. However, this method can only make qualitative recognition and cannot give a quantitative analysis of how certain process affects adsorption kinetics.

More detailed research on the adsorption kinetics of CO_2 by solid amines can be broadly categorized into two groups, i.e. 1) the solid amine particle is treated as an entity; and 2) dual kinetic models are employed.

For the first category(Hou et al., 2021; Vallace et al., 2023; Wang et al., 2016), shrinking core model was used to describe the adsorption process. Adsorption kinetics were mainly influenced by external diffusion, product layer diffusion, and the chemical reaction on the surface of the unreacted core(Hou et al., 2021; Wang et al., 2016). Vallace (Vallace et al., 2023) also treated solid amine particles of several micrometers as a whole. According to his hypothesis, unreacted solid amine particles had high diffusivity such that CO_2 could quickly contact unreacted amines at all locations. Nonetheless, as the reaction proceeded, CO_2 needed to diffuse through the product layer with low diffusivity and only amines near the surface can react with CO_2, which explained a fast and then slow adsorption rate of the adsorption curve. However, this type of model is not consistent with the actual situation, a certain volume of pores still exists in the solid amine adsorbents (Yang et al., 2023), and CO_2 can enter into the solid amine adsorbent through the pores, rather than diffusing through the product layer.

The second category (Ohs et al., 2018; Wang et al., 2020), which posited the existence of two distinct adsorption rates within the solid amine, was first attempted by Bollini (Bollini et al., 2012). The faster rate indicated the reaction of CO_2 with the surface amine, while the slower rate represented the reaction rate of CO_2 with deep-layer amines after diffusing through the surface amine layer (Ohs et al., 2018). Thus, the dual kinetic model could explain the long-tail phenomenon (Jung et al., 2018) which refers to the slow adsorption process during the later stages of adsorption(Wang et al., 2025). However, this model was dependent on hypothesis and failed to establish a connection between the model and the support material structure, lacking detailed calculations and physical substantiation.

From the above discussion, few studies on the CO_2 adsorption kinetics of solid amine adsorbents considered the detailed CO_2 adsorption process, which makes it difficult to understand the evolution of solid amine adsorbents during CO_2 adsorption process. In this paper, a novel adsorption kinetic model has been constructed based on the classical Langmuir adsorption model. The model fits well with experiment data and can be used to explain the effect of temperature and amine loading on the CO_2 adsorption. The model divides amines into two parts: the open amine region and the closed amine region. In the open amine region, the adsorption of CO_2 is not controlled by CO_2 diffusion, so they can maintain a constant and relatively fast adsorption rate, independent of the amine loading. In contrast, CO_2 adsorption in the closed amine region is controlled by CO_2 diffusion, resulting in a significant concentration gradient inside, leading to a slower adsorption rate. By fitting the thermogravimetric curve, parameters such as the ratio of the open amine layer region and the adsorption rate unaffected by diffusion can be obtained. In addition, excessive amine can block the mass transfer channels and eliminate the open amine region. In this case, all CO_2 adsorption is strongly diffusion-limited, resulting in a low apparent adsorption rate.

Nomenclature

Symbol	Meaning	Unit	value	Reference
a	Percentage of amine in the open amine region			
C	CO_2 concentration	mol/m^3		
C_{inner}	Average intra-particle CO_2 concentration due to internal diffusion	mol/m^3		
D	Integrated diffusivity	m^2/s	3.39E-06	Equation S3
$D_{CO2\text{-}N2}$	Diffusivity of CO_2 in nitrogen	m^2/s	1.67E-05	Equation S1
D_e	Effective diffusivity based on particle surface area	m^2/s		
D_{in}	Diffusivity of CO_2 in amines	m^2/s		
dp	Particle diameter	mm	0.855	
J	Diffusion flux	$mol/(m^2 \bullet s)$		
K_0	Initial Langmuir equilibrium constant			
k	Adsorption rate based on adsorbent mass	$m^3/(s \bullet kg)$		
ka	Adsorption rate	$m^3/(s \bullet kg)$		
kd	Desorption rate	$m^3/(s \bullet kg)$		
k_g	Adsorption rate based on adsorbent external surface area	m/s		
kv	Adsorption rate based on adsorbent volume	1/s		
P	Atmospheric pressure	Pa	101325	
q	CO_2 adsorption capacity	mol/kg		
q_e	Equilibrium adsorption capacity	mol/kg		
q_N	N efficiency	mmol CO_2/ mmol N		
q_{total}	Adsorption capacity of the total active sites	mol/kg		
r	Amine radius in the open amine region	m		
R	Gas constant	J/(mol•K)	8.314	
Sh	Sherwood number		2	(Wang et al., 2020)
t	Time	s		
T	Temperature	K		
x_{load}	Mass ratio of amines of adsorbent			
y	The ratio of CO_2 concentration		0.15	
η	Efficiency factor due to internal diffusion			
ρ_{amine}	Amine density	kg/m^3	1030	(Vanini et al., 2023)
ρ_p	Particle density	kg/m^3	890 (0.5R20)	Calculated from experimental data
τ	Tortuosity factor	$1/\varepsilon_p$		(Wang, 2021)
φ_s	Thiele modulus number			
ε_p	Adsorbent porosity		0.15 (0.5R20)	Calculated from experimental data
ΔU	Adsorption heat	J/mol		
Z	Amine length in the closed amine region	m		

Subscript

Symbol	Meaning
i	Time i
N	Based on nitrogen amount
p	Based on particle

2. Materials and methods

2.1. Preparation of PEI loaded resin HP20

Resin HP20 (Diaion, Mitsubishi) with a particle size between 0.8 and 0.9 mm was chosen as supporting material. Took 1 g of the material and degassed it at 110°C for more than three hours. A predetermined mass of Polyethyleneimine (PEI, Molecular weight Mw=600, Purity: 99 %, Aladdin) was added to 10 mL of methanol solution (Purity: 99.9 %, Macklin) and stirred for about 10 min, after which the supporting material was added into the mixture. After continuous stirring at 55°C and a vacuum of 0.5 bar (A) for approximately 2 h, the methanol was nearly evaporated. The remaining substance was taken and placed in a vacuum drying oven over night. The solid amine adsorbent was obtained by further evaporation at 60°C under vacuum for about 1 h. The obtained adsorbents were named as *x*R20, where *x* is the amine loading, representing the weight ratio of PEI in the adsorbent. For example, 0.4R20 represents an amine loading of 0.4.

The performance of different preparation batch is shown in Table 1. The CO_2 adsorption capacity was measured at 90°C by thermogravimetry analysis (TGA, Mettler Toledo TGA 2) as described in the next section, and the amine loading was measured by elemental analysis (Elementar vario MACRO cube). It can be found that the prepared solid amine adsorbents have good repeatability. The actual amine loading is slightly lower than the designed amine loading, which might due to the fact that, during the evaporation of the methanol, some PEI adheres to beaker walls.

2.2. CO_2 adsorption/desorption

CO_2 adsorption capacity was measured by TGA. 4–7 mg solid amine adsorbent particles with an average particle diameter of 0.855 mm were placed in a shallow aluminum crucible with a depth of 1.7 mm to minimize crucible-induced diffusion. The particles were arranged in a monolayer, so that inter-particle diffusion could be neglected. Before the measurement of CO_2 adsorption capacity at different temperatures, the sample was degassed under 100 sccm pure nitrogen at 120°C for about 20 min, during which time the sample mass gradually decreased and remained stable, representing the completion of degassing. After cooling down to the corresponding experimental temperature (30–120°C) at a rate of 5 K/min, the gas flow was switched to 100 sccm of 15% CO_2/N_2 for 20 min to complete the adsorption process. Afterwards, the TGA gas was changed to 100 sccm of pure nitrogen at the same temperature to determine desorption curves. So far, a cycle of CO_2 adsorption/desorption at a certain temperature had been finished. The accuracy of the TGA was verified by measuring a standard adsorbent (Lewatit VP OC 1065) and the results were shown in N.

2.3. The pore volume changes after amine loading

The pore volume changes were measured by ASAP2460 at 77 K to investigate the pore structures of the resin supports and the solid amine adsorbents. Before the measurement, the samples were vacuum degassed at 120°C for one hour. The pore volume at different pore sizes is shown in Figure 1. Detailed data of pore volume are shown in Table S2.

With the increase of amine loading, the pore volume of solid amine adsorbents gradually declines, especially micropores gradually disappear and become blocked. When the amine loading reaches 50%, there are almost no ≤ 20 nm pores remaining. Recently, some studies utilized in situ small-angle neutron scattering (SANS) to survey the pore distribution after PEI loading (Moon et al., 2022; Zhang et al., 2019). They found that the amines preferentially dispersed on the pore surface, and then aggregated in small pores as plugs, which explained the rapid decline of the small pores.

Table 1
CO_2 adsorption capacity and amine loading of three batches of 0.4R20.

Batch	1	2	3
CO_2 adsorption capacity (mmol/g)	2.24	2.24	2.28
Amine loading (%)	39.00	38.08	39.34

2.4. External and internal diffusion in solid amine adsorbent

How CO_2 is adsorbed by solid amine adsorbents is shown in Figure 2 and it includes the following processes: CO_2 firstly diffuses to the particle surface (external diffusion), then CO_2 diffuses inside the pores of the particle (internal diffusion). During the internal diffusion, CO_2 is also adsorbed by amine.

In conjunction with the results of the section 2.3, amine loading on porous materials could be divided into two types: an increase in the thickness of the amine layer in the large pores (open amine region) and the formation of plugs that block small pores (closed amine region). This constitutes two different types of diffusion in the solid amine adsorbent. In the open amine region, CO_2 molecule diffuses in radius direction, from the center of the pore to the amine near the wall. While in the closed amine region, CO_2 molecule diffuses in length direction, from the outside of the plugged amine pore to the inside of the plugged amine pore.

The influence of external diffusion can be represented as:

$$\pi {d_p}^2 k_g \frac{Py}{RT}\left(1-\frac{C_S}{C_G}\right)=\frac{1}{6}\pi {d_p}^3 \rho_p \frac{dq}{dt} \quad (1)$$

where C_s/C_G represents the ratio of the CO_2 concentration at particle surface to the CO_2 concentration in surrounding gas. The closer the value is to 1, the less the influence of external diffusion. The external mass transfer coefficient k_g is calculated as:

$$k_g=\frac{\mathrm{Sh}\cdot D_{CO_2-N_2}}{d_p} \quad (2)$$

The Thiele modulus (Sharratt and Mann, 1987) is used to describe

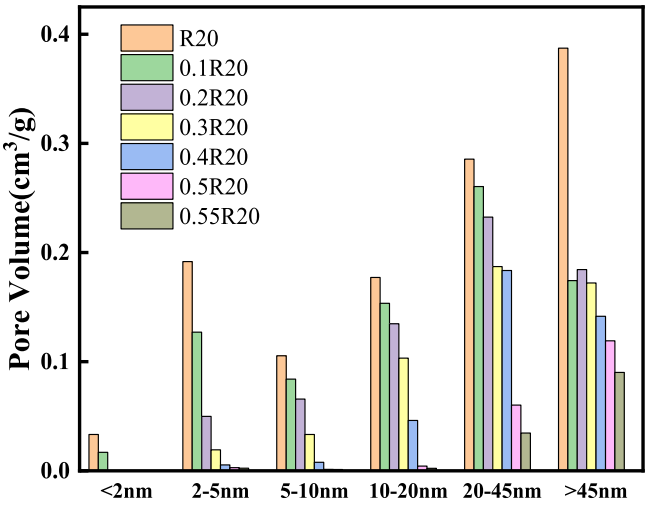

Fig 1. Variation of pore volume of solid amine adsorbents with amine loading.

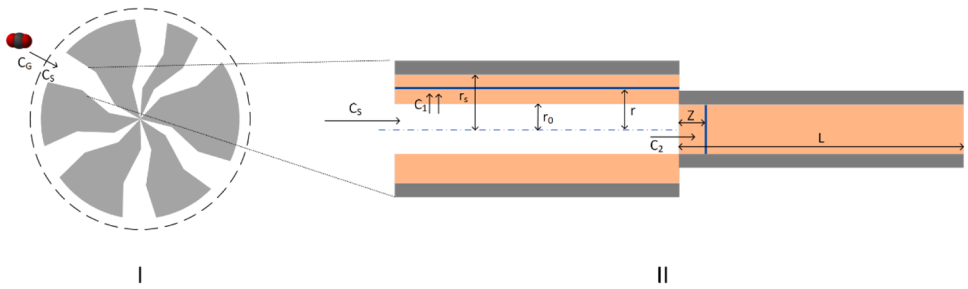

Fig 2. Illustration of CO_2 adsorption process. (I) external and internal diffusion of solid amine adsorbent particle. (II) the CO_2 diffusion in open amine region and closed amine region, where the blue region means the infinitesimal region of governing equation.

the impact of internal diffusion, which can be calculated as:

$$\varphi_s = \frac{d_p}{6}\sqrt{\frac{k_v}{D_e}} \tag{3}$$

where k_v is the adsorption rate based on adsorbent volume and can be calculated by equation (4). D_e is the effective diffusivity based on particle surface area, as expressed in equation (5).

$$k_v = \rho_p \frac{dq}{dt} \Big/ C_S \tag{4}$$

$$D_e = D\frac{\varepsilon_p}{\tau} \tag{5}$$

The efficiency factor η due to internal diffusion can be obtained as:

$$\eta = \frac{C_{inner}}{C_S} = \frac{1}{\varphi_s}\left[\frac{1}{\tanh(3\varphi_s)} - \frac{1}{3\varphi_s}\right] \tag{6}$$

2.5. Dual-region kinetic model

The CO_2 adsorption in the amine region can be divided into two parts, as shown in equation (7).

$$q = a * q_{open} + (1-a)q_{close} \tag{7}$$

For open amine region, the governing equation is shown as:

$$2\pi r J_r - 2\pi(r+\Delta r)J_{r+\Delta r} = 2\pi r \Delta r\left(\frac{\rho_{amine}}{x_{load}}\frac{dq}{dt} + \frac{\partial C}{\partial t}\right) \tag{8}$$

where J_r means the diffusion flux at the radius of r and can be determined as:

$$J_r = -D_{in}\frac{\partial C}{\partial r} \tag{9}$$

Combining equation (8) and (9), equation (10) can be deduced as:

$$\frac{D_{in}}{r}\left(r\frac{\partial^2 C}{\partial r^2} + \frac{\partial C}{\partial r}\right) = \frac{\rho_{amine}}{x_{load}}\frac{dq}{dt} + \frac{\partial C}{\partial t} \tag{10}$$

The boundary conditions are:

$$\begin{cases} r = r_0, C = C_1 \\ r = r_s, \dfrac{\partial C}{\partial r} = 0 \end{cases} \tag{11}$$

where all of the above symbols are graphically shown in Figure 2.

Similarly, the continuity equation in the closed amine region can be derived as:

$$D_{in}\frac{\partial^2 C}{\partial Z^2} = \frac{\rho_{amine}}{x_{load}}\frac{dq}{dt} + \frac{\partial C}{\partial t} \tag{12}$$

The corresponding boundary conditions are:

$$\begin{cases} Z = 0, C = C_2 \\ Z = L, \dfrac{\partial C}{\partial r} = 0 \end{cases} \tag{13}$$

where all of the above symbols are also represented in Figure 2.

In equation (10) and (12), the adsorption term can be derived from the Langmuir adsorption model (Lv et al., 2024), the classical adsorption model is shown as:

$$\frac{dq}{dt} = k_a C\left(1 - \frac{q}{q_{total}}\right) - k_d\frac{q}{q_{total}} \tag{14}$$

Then equation (14) can be changed into:

$$\frac{dq}{dt} = kC\left(1 - \frac{q}{q_e}\right) \tag{15}$$

where,

$$\begin{cases} k = \dfrac{k_a C + k_d}{C} \\ q_e = \dfrac{k_a q_{total} C}{k_a C + k_d} \end{cases} \tag{16}$$

Since C in equation (15) is not a constant, the differential equation cannot be solved directly. Thus, equation (15) should be solved by finite difference method:

$$\frac{dq_i}{dt} = \frac{q_i - q_{i-1}}{\Delta t} = kC_{i-1}\left(1 - \frac{q_{i-1}}{q_e}\right) \tag{17}$$

The q at time i can always be calculated by C and q at time i-1. By combining Equation (17) with Equation (10) and (12), C and q can be determined at any position and at any moment. The equations were solved using MATLAB 2021a, and the fitting to the thermogravimetric curves was implemented with the lsqcurvefit function in MATLAB.

The following assumptions were set: 1. Ideal gas; 2. CO_2 adsorption by amine conformed to Langmuir adsorption model; 3. Pores in the closed amine region were isometric and the radial variations were neglected; 4. CO_2 adsorption rate and CO_2 diffusion in the amine did not vary with position.

2.6. CO_2 diffusivity in PEI

It is important for the kinetic model to determine the CO_2 diffusivity in PEI. However, to the best of our knowledge, the diffusivity in PEI has not been measured directly in experiments. Diffusivity of similar materials have been measured. Li (Li et al., 2015) doped PEI into polyethylene glycol to prepare a film, which had a CO_2 diffusivity about 1.25E-10 m^2/s. Hu (Hu et al., 2006) reported a CO_2 diffusivity in PEG-2000 grafted P[MATMA][BF4] membranes of 1.9 E-11 m^2/s. Baumann [37] determnined the self-diffusivity of PEI using the quasi-elastic neutron scattering as 1.5E-12 m^2/s and found that the self-diffusivity of PEI increased with adsorption of CO_2 and water. Other

researchers used molecular dynamics (MD) to estimate the CO_2 diffusivity in PEI. Turgman (Turgman-Cohen et al., 2015) applied the amount of zwitterion to represent the state of the amine after CO_2 adsorption. With the increase of the amount of zwitterion, CO_2 diffusivity declined dramatically from 1E-7 to 1E-9 m^2/s. Narimani (Narimani et al., 2017) calculated the CO_2 diffusivity of four amines by MD simulations, which was about 6E-10 m^2/s. From the above analysis, CO_2 diffusivity in PEI has a great probability to be greater than 1E-12 m^2/s, which was used in subsequent calculations. The extreme conditions were considered to determine whether the CO_2 adsorption was affected by diffusion.

3. Results and Discussions

3.1. The effect of temperature

Figure 3 (a) shows the adsorption curves of 0.5R20 at different temperatures. With temperature increasing, the CO_2 adsorption capacity gradually decreases as shown in Figure 3 (b). It can be observed that the variation could be fitted by equation (18) derived from equation (14). The fitting result is shown in the figure.

$$q_T = q_{total}\frac{K_0 \exp\left(\frac{\Delta U}{RT}\right)C}{1 + K_0 \exp\left(\frac{\Delta U}{RT}\right)C} \tag{18}$$

At lower temperatures (<70°C), the adsorption has not reached equilibrium during the experiment period, the CO_2 adsorption capacity is still slowly increasing after 20 min, demonstrating a long-tail phenomenon (Jung et al., 2018). In addition, the difference in adsorption capacity is small within the temperature range. While at higher temperatures, the adsorption capacity decreased with increasing temperature but reached equilibrium quickly. The CO_2 adsorption capacity at different temperatures fitted well with equation (18), indicating that the adsorption mechanism of solid amine adsorbent is consistent with Langmuir adsorption model.

Desorption curves of 0.5R20 at different temperatures are shown in Figure 4. The desorption rate as well as the desorption extent (the ratio of desorption capacity to adsorption capacity) increases gradually with increasing temperature. Some researchers defined the desorption extent as the percentage of physical adsorption (Yang et al., 2024), which represents the desorption capacity that can be achieved at a given temperature by changing only the gas flow. When temperature exceeds 90°C, the desorption rate increases dramatically, and all of the adsorbed CO_2 could be desorbed within 20 min, exhibiting characteristics of traditional physical adsorbents. Furthermore, in combination with equation (16), the fast desorption rate could explain the rapid decrease in CO_2 adsorption capacity at temperatures over 90°C.

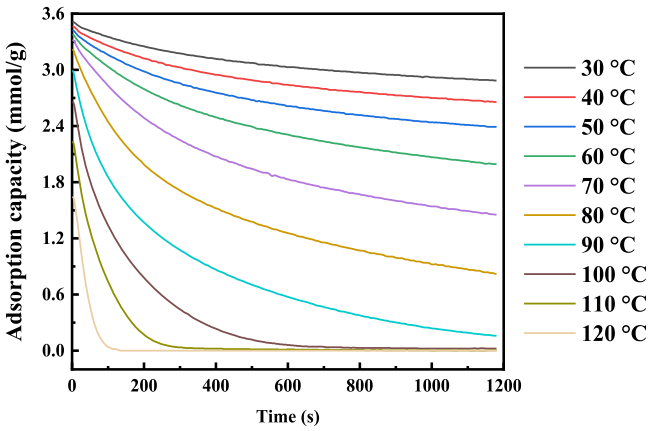

Fig 4. Desorption curves of 0.5R20 at different temperatures.

3.2. The effect of amine loading

At lower amine loadings, adsorption capacity increases almost linearly with the increasing loading. However, when amine loading reaches 0.55, which exceeds the theoretical maximum loading of 0.53 as calculated in equation (19), the adsorption capacity conversely decreases as the amine loading arises. Figure 5 (b) shows the Adsorption curves at different amine loadings. Unlike the smaller amine loading, at the amine loading of 0.55, the adsorption rate significantly reduces, as evidenced by a notable rightward shift of the adsorption curve and the adsorption capacity is far from reaching equilibrium within 20 min.

$$\text{theoreticalmaximumloading} = \frac{V_{total}}{\rho_{amine}} \tag{19}$$

The CO_2 adsorption capacity based on the nitrogen amount (N efficiency) is obtained by dividing the CO_2 adsorption amount by the nitrogen content. The value represents how many moles of CO_2 can be adsorbed by per mole of amino, and the theoretical maximum value is 0.5, since the existing mechanisms indicate that it takes two aminos to adsorb one CO_2. The N efficiency at different temperatures is shown in Figure 6.

Unlike the case at lower amine loadings, when the amine loading reach 0.55, the nitrogen efficiency tends to first increase and then decrease with increasing temperature. The results are in agreement with results in the literatures (Lin et al., 2023; Shen et al., 2022), adsorbents with larger N efficiency need higher temperature to achieve peak

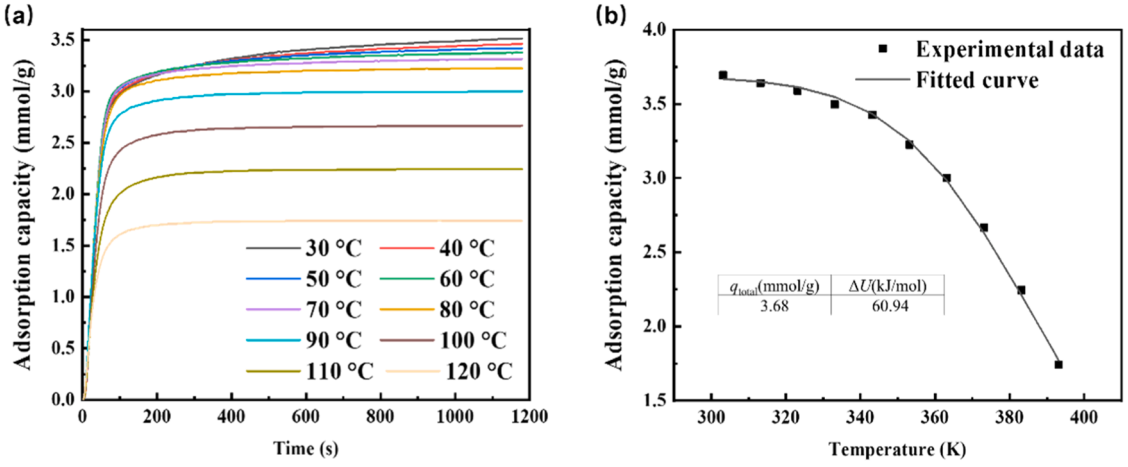

Fig 3. (a) Adsorption curves of 0.5R20 at different temperatures. (b) Variety of adsorption capacity with temperature.

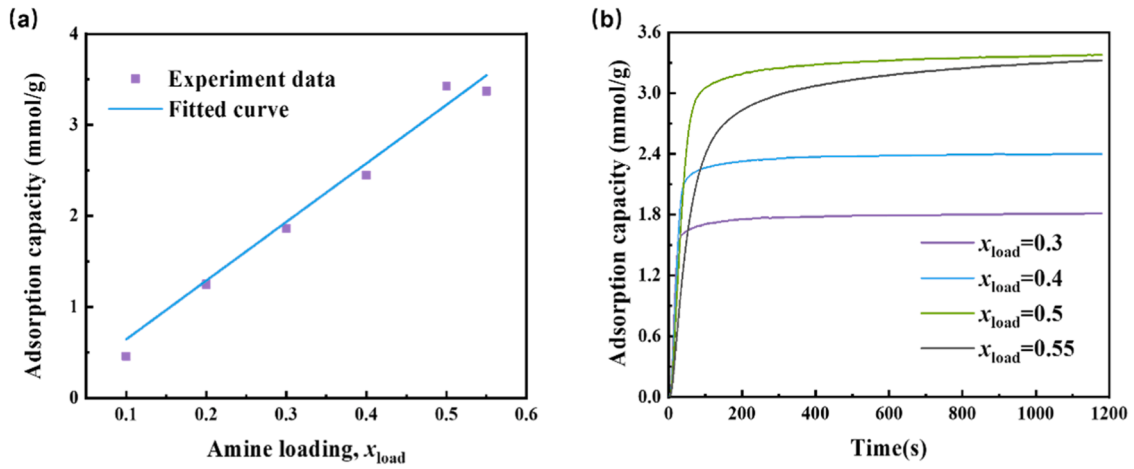

Fig 5. (a) The variety of CO_2 adsorption capacity (60°C, 20 min) with amine loading. (b) Adsorption curves at different amine loadings at 60°C.

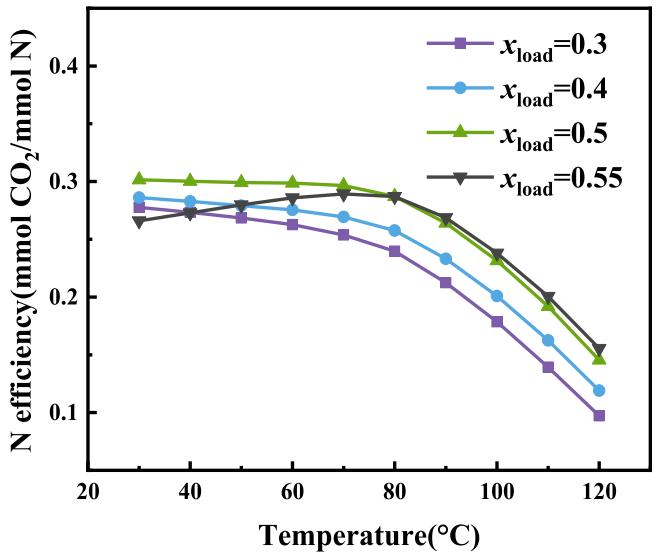

Fig 6. The variety of N efficiency with temperature.

adsorption capacity. In addition, the N efficiency increases as the amine loading rises. The difference in N efficiency of adsorbents with different amine loading at higher temperatures is further widened. It can be found that the N efficiency decreases gradually from 30°C at the amine loading of 0.3 and 0.4. Whereas when the amine loading is 0.5, the adsorption capacity decreases significantly only above 70°C. The adsorbents with larger amine loading have better resistance to high temperatures and are more suitable for use at higher temperatures.

3.3. *The external and internal diffusion*

Since the parameters involved in the calculation of internal and external diffusion, such as CO_2 concentration and diffusion coefficient, vary with temperature. The most extreme conditions are often used to determine whether internal and external diffusion need to be considered in the construction of the kinetic model. Combined with the equation (1), (2) and (S1), the effect of external diffusion gradually increases with decreasing temperature. The adsorption temperature of 30°C was selected for the calculation, the variation of C_s/C_G with time is shown in Figure 7 (a).

The adsorption rate decreases with increasing adsorption time, while the value of C_s/C_G shows the opposite trend. Even at 0 s, the decrease in C_s due to external diffusion is small. Therefore, the change in CO_2 concentration due to the external diffusion can be negligible.

Due to the large adsorption rate at the early time, the effect of the internal diffusion is severe, as shown in Figure 7 (b). At 0 s, the efficiency factor η is only 0.32, indicating that the average CO_2 concentration within the adsorbent is significantly lower than the surrounding concentration. As the adsorption proceeds, the adsorption rate decreases rapidly, η gradually approaches 1, at which time the CO_2 concentration within the adsorbent gradually matches that of the surrounding

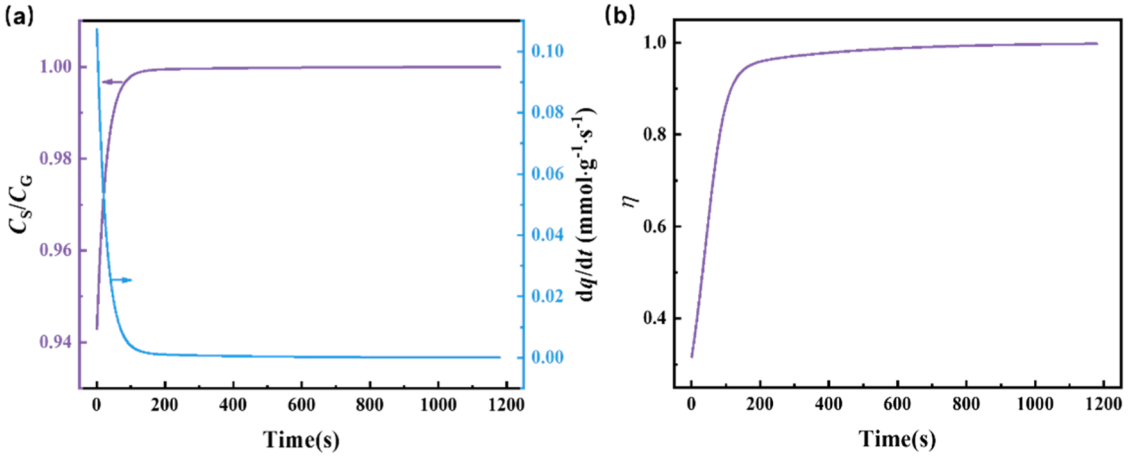

Fig 7. (a) The variety of adsorption rate and adsorbent surface concentration with time. (b) The variety of efficiency factor η due to the internal diffusion with time.

atmosphere, and thus internal diffusion does not affect the equilibrium adsorption capacity. In the calculation of subsequent kinetic model, the effect of internal diffusion must be considered.

3.4. Dual-region model

In the open amine region, CO_2 diffuses from the center of the pore to the amine near the surface of supporting materials. As shown in Figure 1, Amines are mainly distributed in pores smaller than 45 nm, so r_s in the model is taken as 25 nm. The CO_2 diffusivity is set as 1E-12 m^2/s, which is the minimum value as discussed in section 2.6. The extreme conditions were considered to determine whether the CO_2 adsorption in the open amine region was affected by diffusion.

The variation of CO_2 concentration in the open amine region with the radius r is plotted as shown in Figure 8 (a). It can be seen that at t=0.001 s, there is a large concentration gradient within the amine layer due to the initial diffusion, and the CO_2 concentration near the wall is low. After that, the concentration gradient decreases rapidly due to the consumption by the reaction. The concentration gradient at t=0.01 s and t=0.1 s almost completely overlap. The average concentration in the open amine region is 97.6% of that on the outside of the amine layer at t=0.01 s. Therefore, it can be inferred that diffusion in the region of the open amine layer has almost no effect on the adsorption kinetic of the solid amine adsorbents. The CO_2 adsorption process in the region is mainly controlled by the adsorption rate, which can be directly expressed by equation (17).

For CO_2 adsorption in the closed amine region, the partial differential equation (12) should be solved. By fitting to the thermogravimetric curves, the four parameters a, k_N, D_{in}, and L can be obtained. The parameters D_{in} and the closed amine layer length L are strongly correlated and both are difficult to obtain by experiment. The value of L was fitted to 2.5 μm to ensure that D_{in} was distributed between 10^{-12} and 10^{-10} m^2/s, thus maintaining the same magnitude as the data discussed in the section 2.6. Figure 8 (b) exhibits the variation of CO_2 concentration and CO_2 adsorption capacity with length in the closed amine region at 20 min. Due to the diffusion control, a significant concentration gradient remains in the closed amine region at 20 minutes, some of amines have not yet reached adsorption equilibrium. As the adsorption time increases, the adsorption front gradually propagates to deeper amine, resulting in the phenomenon shown in Figure 3 (a) where the adsorption capacity continues to rise slowly even after 20 minutes at low temperatures. The CO_2 concentration gradient is more pronounced than the adsorption capacity gradient because CO_2 is not only adsorbed by amines but also needs to diffuse to deeper amines.

The fitting result of dual-region model is shown in Figure 9(a). It can be found that the dual-region model can fit the experimental curve more accurately compared to the pseudo-first order kinetic model. The pseudo-first order kinetic model tends to overestimate the adsorption rate. The dual-region model can obtain the proportion of open amine region from the experimental curves, and thus shows different adsorption stages: in the early stage of adsorption, CO_2 adsorption in the open amine region is not affected by diffusion, CO_2 adsorption proceeds rapidly and reaches equilibrium quickly. Whereas for amine in the closed amine region, the rate of CO_2 exposure to amine is slow due to the significant influence of diffusion. It takes long time for the amines to adsorb CO_2.

To account for the effect of amine loading and temperature, the parameters a, k_N and D_{in} at the amine loading of 0.3–0.5 and the temperature of 30–120°C are shown in Figure 9 (b)-(d).

The percentage of open amine region a, does not change a lot at the amine loading of 0.3–0.5. With the increase of temperature, a firstly increases and then decreases, which is due to the balance of two effects: on the one hand, with the increase of temperature, the diffusivity of CO_2 within the amines increases. More amines present the characteristics of the open amine region, which are not affected by the diffusion of CO_2. On the other hand, at higher temperatures, CO_2 desorption rate in the closed amine region is slow due to the long diffusion path, thus retaining a high CO_2 adsorption capacity as presented in equation (16). CO_2 adsorption in the open amine region decreases rapidly with increasing temperature, whereas closed amine region is less sensitive to temperature. Amines in the closed region remain high CO_2 adsorption capacity at high temperature, thus exhibiting smaller a. At high temperature of 110 and 120°C, a will rise instead because the adsorption rate in the open amine region decreases sharply at high temperatures, as shown in Figure 9 (c), while the slow adsorption rate in the closed amine region will increase due to the increase of CO_2 diffusivity. The two adsorption rates gradually converge, demonstrating the disappearance of dual-region phenomenon.

Figure 9(c) shows the variety of k with temperature at different amine loadings. When the amine loading is between 0.3 and 0.5, the adsorption rate k is almost the same, as shown in Figure 5 (b), where the adsorption curves almost overlap when the amine loading is between 0.3 and 0.5. The adsorption rate k is independent of amine loading, indicating that there is an area in the solid amine that is not diffusion-controlled. When the temperature is below 80°C, k also does not change significantly, as shown in Figure 3 (a). As the adsorption temperature continues to rise, k decreases rapidly, consistent with the rapid decrease in CO_2 adsorption capacity. k of 0.5R20 exceeds that of adsorbents with low amine loading at high temperatures. It is worth noting that, as shown in equation (15), adsorption rate k here includes the effect of adsorption capacity. Therefore, the value can not only indicate the time required for reaching the adsorption capacity equilibrium, but

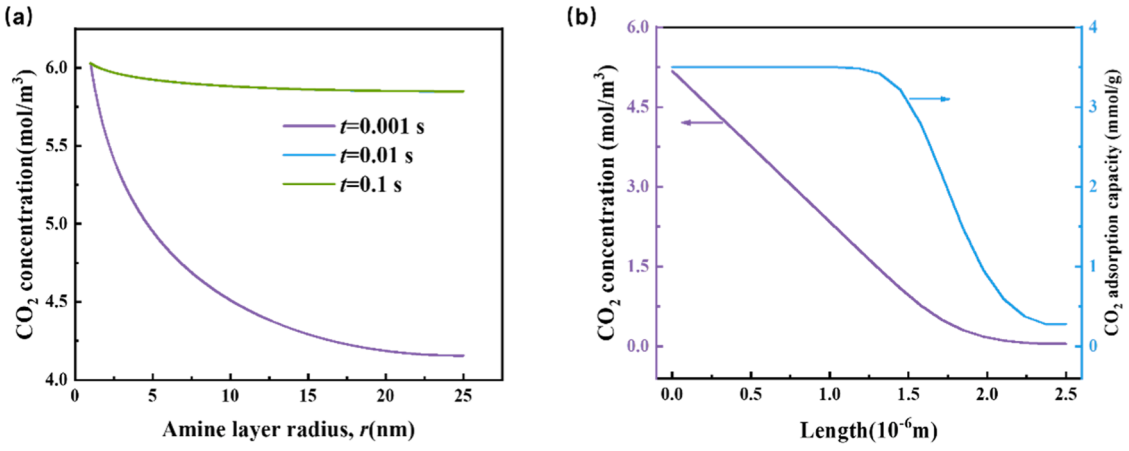

Fig 8. (a) The variation of CO_2 concentration in the open amine region with the radius r. (b) Variation of CO_2 concentration and CO_2 adsorption capacity with length in the closed amine region at 20 min.

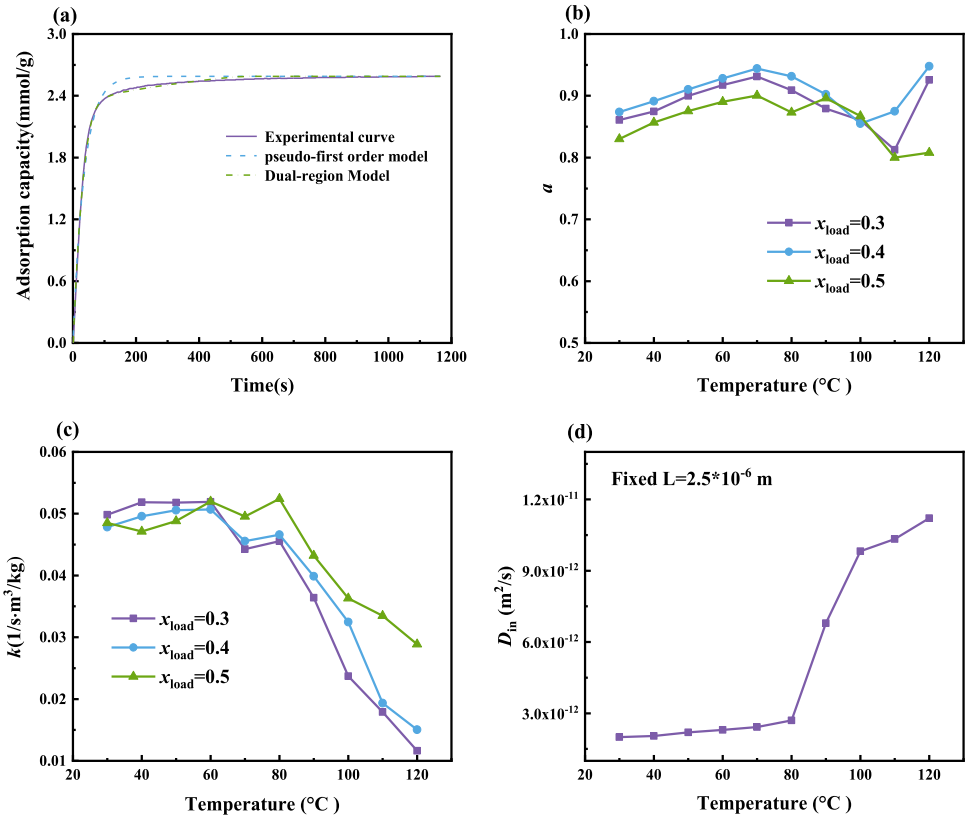

Fig 9. (a) Experimental curves and fitting results for 0.5R20 at 80°C. (b) The variety of a with temperature at different amine loadings. (c) The variety of k with temperature at different amine loading. (d) The variety of D_{in} with temperature.

also is a comprehensive parameter to reflect the time to achieve a certain CO_2 adsorption capacity. For CO_2 adsorption at high temperatures, 0.5R20 is more recommended.

Further increasing the amine loading to 0.55, the adsorption rate shows a great decrease, as shown in Figure 5 (b). While based on the dual-region model, the adsorption rate within the open amine region remains constant and independent of amine loading. Therefore, amines of amine loading of 0.55 have accumulated excessively, completely blocking the mass transfer channels, there is no longer open amine regions. The phenomenon can also be observed in the SEM images, as shown in Figure S1. when the amine loading is 0.55, the surface becomes smoother, excess amine covers the particle surface, as reported by (Wang et al., 2014; Wang et al., 2013). All CO_2 adsorption by amines is diffusion-limited, exhibiting a low apparent adsorption rate.

The CO_2 diffusivity in amines, as shown in Figure 9(d), has clear trends: D_{in} increases with the increase of temperature. And when the temperature exceeds 70°C, D_{in} increases sharply, which is consistent with the results in Figure 3(a), at temperature above 70°C, the CO_2 adsorption capacity can reach equilibrium within 20 min. The result is also consistent with (Zhang et al., 2019), which found that the size of the intramolecular voids between PEI chains had no change from 25 to 75°C but expanded from 75 to 120°C. It is worth noting that the D_{in} value in this paper is not a real value; it is obtained by fitting based on a fixed L of 2.5 μm. L and D_{in} are strongly correlated. They jointly determine the proportion of amines in the closed amine region that can contact and adsorb CO_2 within a certain period of time.

3.5. Discussion

The model not only helps us to understand the CO_2 adsorption process, but also guides the design of adsorbents. The amines in the open region are less constrained by CO_2 diffusion, so measures can be taken to increase the percentages of the open amine region. Selection of supporting materials with larger pore sizes is one way, since larger pore sizes often correspond to smaller L in Figure 2. Some studies have found the same results. At the same amine loading, adsorbents with high pore sizes always have high adsorption rate (Wang et al., 2014). Zhang (Zhang et al., 2014) prepared a series of MCF supporting materials with different pore sizes and found that, at the same amine loading, the CO_2 adsorption capacity of adsorbents with smaller pore sizes was extremely low at low temperatures, whereas adsorbents with the larger pore sizes could achieve higher CO_2 adsorption capacity due to better amine distribution. With the decrease of pore sizes, adsorbents required higher temperatures to reach peak adsorption capacity (Lin et al., 2024). In addition, the model could explain the effect of amine type on the CO_2 adsorption. Zang (Zang et al., 2024) found that amines with high CO_2 diffusivity were favorable for achieving peak adsorption capacity at low temperatures. This was because the amines with high CO_2 diffusivity

Table 2
Common kinetic model used for solid amine adsorbents.

Kinetic model	Equation	Reference
Pseudo-first order model	$\frac{dq}{dt} = k(q_e - q_t)$	(Loganathan et al., 2014)
Pseudo-second order model	$\frac{dq}{dt} = k(q_e - q_t)^2$	(Ho and McKay, 1998)
Avrami's fractional order model	$\frac{dq}{dt} = k^n t^{n-1}(q_e - q_t)$	(Avrami, 1939)
double-exponential model	$q_t = q_e - \frac{D_1}{m_a}\exp(-k_1 t) - \frac{D_2}{m_a}\exp(-k_2 t)$	(Wilczak and Keinath, 1993)
Boyd's film-diffusion model	$F = 1 - \frac{6}{\pi^2}\sum_{n=1}^{\infty}\frac{1}{n^2}\exp(-n^2 B_t)$	(Boyd et al., 1947)
Intraparticle diffusion model (Weber-Morris model)	$q_t = k_{id}t^{1/2} + C$	(Morris and Weber, 1964)

could more fully utilize the amines in the closed region.

There are already many adsorption models, as shown in Table 2. Among the common kinetic models, Boyd's film-diffusion model and Weber-Morris model mainly evaluate whether film diffusion or intra-particle diffusion is the single rate-limiting step. Pseudo-first order model, Pseudo-second order model, Avrami's fractional order model are commonly used to fit the adsorption curve of CO_2 adsorption by solid amine adsorbents, and they can qualitatively reflect the adsorption mechanism. For example, the pseudo-second order model is often used in chemical adsorption, while the coefficient n in Avrami's fractional order model reflects the growth pattern of the adsorption product (Yang et al., 2022). However, none of the above models can consider the diffusion limitation within the amine. The dual-region model quantitatively considers film diffusion, internal diffusion and CO_2 diffusion in the amine layer, and ultimately obtains a good fitting result. The dual-region model is similar in form to the double-exponential model, but explains the reasons for the occurrence of rapid adsorption rates and slow adsorption rates.

There are many factors that may affect the applicability of the model, such as amine type, support materials, CO_2 partial pressure and humidity. Figure S2 shows CO_2 adsorption curves at a CO_2 partial pressure of 1 bar. Figure S3 shows CO_2 adsorption curves under different amine types (TEPA, PEI600, PEI-1800, and PEI-10000) and different support materials, and the fitting results is shown in Table S3, Table S4 and Table S5. All the above CO_2 adsorption curves obey dual-region model: At low temperatures, CO_2 adsorption curves have an obvious long-tail effect. When the amine loading is extremely high, the adsorption capacity and adsorption rate decrease significantly due to strong diffusion control. Figure S4–S6 shows the CO_2 breakthrough curves under different moisture contents and adsorption temperatures. It can be found that moisture does not significantly affect the adsorption curve. Therefore, none of the above parameters will affect the model applicability.

4. Conclusion

In this study, the effects of temperature and amine loading on CO_2 adsorption by solid amine adsorbents were experimentally investigated, and then a dual-region kinetic model was constructed by analyzing the external diffusion, internal diffusion and the diffusion inside the amine layer. Finally, the effects of temperature and amine loading on CO_2 adsorption were explained by the model. The following conclusions are obtained:

The CO_2 adsorption by solid amine adsorbents below 70°C has an obvious long-tail effect, and the adsorption capacity is far from reaching equilibrium in 20 min. When the amine loading is less than 0.5, the adsorption capacity and the N efficiency gradually decrease with decreasing amine loading and increasing temperature. While the amine loading reaches 0.55, the adsorption capacity is instead lower than that of 0.5R20. For 0.55R20, a high temperature (80°C) is required to reach the peak adsorption capacity.

CO_2 adsorption is almost unaffected by the external diffusion and the diffusion in the open amine region, but it is significantly affected by internal diffusion. The CO_2 adsorption in the closed amine region is the main reason for the long-tail effect. When the amine loading is less than 0.5, the CO_2 adsorption rate is almost the same. While the amine loading reaches 0.55, the CO_2 adsorption rate greatly decreases due to blockage of diffusion pores.

CRediT authorship contribution statement

Shun Wang: Writing – original draft, Software, Investigation, Formal analysis, Conceptualization. **Mengyin Xie:** Writing – original draft, Methodology, Conceptualization. **Shujuan Wang:** Writing – review & editing, Supervision, Investigation, Conceptualization. **Yuqun Zhuo:** Writing – review & editing, Supervision, Project administration, Formal analysis, Conceptualization.

Declaration of competing interest

The authors declare that they have no known competing financial interests or personal relationships that could have appeared to influence the work reported in this paper.

Acknowledgements

This work was supported by "the Fundamental Research Funds for the Central Universities (No. 2022ZFJH004).

Supplementary materials

Supplementary material associated with this article can be found, in the online version, at doi:10.1016/j.ccst.2025.100491.

Reference

Avrami, M., 1939. Kinetics of phase change. I General theory. J Chem Phys 7 (12), 1103–1112. https://doi.org/10.1063/1.1750380.
Birol, F., 2023. World Energy Outlook 2023. International Energy Agency.
Bollini, P., Brunelli, N.A., Didas, S.A., Jones, C.W., 2012. Dynamics of CO2 adsorption on Amine Adsorbents. 2. Insights into adsorbent design. Ind Eng Chem Res 51 (46), 15153–15162. https://doi.org/10.1021/ie3017913.
Bos, M.J., Kreuger, T., Kersten, S.R.A., Brilman, D.W.F., 2019. Study on transport phenomena and intrinsic kinetics for CO2 adsorption in solid amine sorbent. Chem. Eng. J. 377, 120374. https://doi.org/10.1016/j.cej.2018.11.072.
Boyd, G.E., Schubert, J., Adamson, A.W., 1947. The exchange adsorption of ions from aqueous solutions by Organic Zeolites. I. Ion-exchange Equilibria1. J. Am. Chem. Soc 69 (11), 2818–2829. https://doi.org/10.1021/ja01203a064.
Carlson, C.J., Albery, G.F., Merow, C., Trisos, C.H., Zipfel, C.M., Eskew, E.A., Olival, K.J., Ross, N., Bansal, S., 2022. Climate change increases cross-species viral transmission risk. Nature. https://doi.org/10.1038/s41586-022-04788-w.
Chuah, C.Y., Ho, Y.L., Syed, A.M.H., Thivyalakshmi, K.G.K., Yang, E., Johari, K., Yang, Y., Poon, W.C., 2025. Applicability of adsorbents in direct air capture (DAC): recent progress and future perspectives. Ind Eng Chem Res 64 (8), 4117–4147. https://doi.org/10.1021/acs.iecr.4c03265.
Dale, S., 2022. Statistical Review of World Energy. BP p.l.c.
Daryayehsalameh, B., Nabavi, M., Vaferi, B., 2021. Modeling of CO2 capture ability of [Bmim][BF4] ionic liquid using connectionist smart paradigms. Environ. Technol. Innov. 22, 101484. https://doi.org/10.1016/j.eti.2021.101484.
Ho, Y.S., McKay, G., 1998. Sorption of dye from aqueous solution by peat. Chem. Eng. J. 70 (2), 115–124. https://doi.org/10.1016/S0923-0467(98)00076-1.
Hou, C., Kumar, D.R., Jin, Y., Wu, Y., Lee, J.J., Jones, C.W., Wang, T., 2021. Porosity and hydrophilicity modulated quaternary ammonium-based sorbents for CO2 capture. Chem. Eng. J. 413, 127532. https://doi.org/10.1016/j.cej.2020.127532.
Hu, E., Lin, L., Chen, K., Li, J., Gao, Y., Chang, J., Qin, W., Zhao, Y., Jiang, J., 2025. CO2 Capture using resin-based solid amines: characteristic, application, regeneration and deactivation mechanism. Sep Purif Technol 360, 131125. https://doi.org/10.1016/j.seppur.2024.131125.
Hu, X., Tang, J., Blasig, A., Shen, Y., Radosz, M., 2006. CO2 permeability, diffusivity and solubility in polyethylene glycol-grafted polyionic membranes and their CO2 selectivity relative to methane and nitrogen. J Memb Sci 281 (1), 130–138. https://doi.org/10.1016/j.memsci.2006.03.030.
Jung, W., Park, J., Lee, K.S., 2018. Kinetic modeling of CO2 adsorption on an amine-functionalized solid sorbent. Chem Eng Sci 177, 122–131. https://doi.org/10.1016/j.ces.2017.11.003.
Li, X., Cheng, Y., Zhang, H., Wang, S., Jiang, Z., Guo, R., Wu, H., 2015. Efficient CO2 capture by functionalized graphene oxide nanosheets as fillers to fabricate multi-permselective mixed matrix membranes. ACS Appl Mater Interfaces 7 (9), 5528–5537. https://doi.org/10.1021/acsami.5b00106.
Lin, L., Han, S., Meng, F., Li, J., Chen, K., Hu, E., Jiang, J., 2024. The influence of pore size and pore structure of silica-based material on the amine-modified adsorbent for CO2 capture. Sep Purif Technol 340, 126735. https://doi.org/10.1016/j.seppur.2024.126735.
Lin, L., Ju, T., Han, S., Meng, F., Li, J., Jiang, J., 2023. Comparison of characteristics and performance between PEI and DETA impregnated on SBA-15 for CO2 capture. Sep Purif Technol 322, 124346. https://doi.org/10.1016/j.seppur.2023.124346.
Liu, Q., Shi, J., Zheng, S., Tao, M., He, Y., Shi, Y., 2014. Kinetics studies of CO2 adsorption/desorption on amine-functionalized multiwalled carbon nanotubes. Ind Eng Chem Res 53 (29), 11677–11683. https://doi.org/10.1021/ie502009n.
Loganathan, S., Tikmani, M., Edubilli, S., Mishra, A., Ghoshal, A.K., 2014. CO2 adsorption kinetics on mesoporous silica under wide range of pressure and temperature. Chem. Eng. J. 256, 1–8. https://doi.org/10.1016/j.cej.2014.06.091.
Lv, Y., Cheng, K., Gao, J., Sun, W., Luo, Q., Li, Y., Deng, Z., Lai, R., Wu, W., Dai, Z., Ma, F., 2024. Corrosion resistance of Nb and NbTi alloy predicted by hydrogen evolution reaction models modified with Langmuir isotherm adsorption theory. Mater Chem Phys 319, 129386. https://doi.org/10.1016/j.matchemphys.2024.129386.

Meng, R., Jiang, Y., Jiang, J., Liu, J., Kong, C., Zhang, Z., 2025. Macroscopic mechanism of amine solution regeneration enhanced by 3D printed monolithic kaolin catalyst. Fuel 391, 134727. https://doi.org/10.1016/j.fuel.2025.134727.

Moon, H.J., Carrillo, J.-M., Leisen, J., Sumpter, B.G., Osti, N.C., Tyagi, M., Jones, C.W., 2022. Understanding the impacts of support–Polymer interactions on the dynamics of poly(ethyleneimine) confined in mesoporous SBA-15. J. Am. Chem. Soc 144 (26), 11664–11675. https://doi.org/10.1021/jacs.2c03028.

Morris, J.C., Weber, W.J., 1964. Removal of biologically-resistant pollutants from waste waters by adsorption. In: Southgate, B.A. (Ed.), Advances in Water Pollution Research. Pergamon, pp. 231–266. https://doi.org/10.1016/B978-1-4832-8391-3.50032-4.

Narimani, M., Amjad-Iranagh, S., Modarress, H., 2017. Performance of tertiary amines as the absorbents for CO2 capture: quantum mechanics and molecular dynamics studies. J Nat Gas Sci Eng 47, 154–166. https://doi.org/10.1016/j.jngse.2017.09.009.

Ohs, B., Krödel, M., Wessling, M., 2018. Adsorption of carbon dioxide on solid amine-functionalized sorbents: A dual kinetic model. Sep Purif Technol 204, 13–20. https://doi.org/10.1016/j.seppur.2018.04.009.

Sayari, A., Belmabkhout, Y., Serna-Guerrero, R., 2011. Flue gas treatment via CO2 adsorption. Chem. Eng. J. 171 (3), 760–774. https://doi.org/10.1016/j.cej.2011.02.007.

Serna-Guerrero, R., Sayari, A., 2010. Modeling adsorption of CO2 on amine-functionalized mesoporous silica. 2: kinetics and breakthrough curves. Chem. Eng. J. 161 (1), 182–190. https://doi.org/10.1016/j.cej.2010.04.042.

Sharratt, P.N., Mann, R., 1987. Some observations on the variation of tortuosity with thiele modulus and pore size distribution. Chem Eng Sci 42 (7), 1565–1576. https://doi.org/10.1016/0009-2509(87)80161-6.

Shen, X., Yan, F., Li, C., Qu, F., Wang, P., Zhao, S., Zhang, Z., 2022. Amine-functionalized nano-Al2O3 adsorbent for CO2 separation from biogas: efficient CO2 uptake and high anti-urea stability. J Clean Prod 332, 130078. https://doi.org/10.1016/j.jclepro.2021.130078.

Siegelman, R.L., Kim, E.J., Long, J.R., 2021. Porous materials for carbon dioxide separations. Nat Mater 20 (8), 1060–1072. https://doi.org/10.1038/s41563-021-01054-8.

Szima, S., Nazir, S.M., Cloete, S., Amini, S., Fogarasi, S., Cormos, A.-M., Cormos, C.-C., 2019. Gas switching reforming for flexible power and hydrogen production to balance variable renewables. Renew. Sustain. Energy Rev. 110, 207–219. https://doi.org/10.1016/j.rser.2019.03.061.

Tang, W., Liu, T., Gao, H., Wang, S., Zhou, M., Yu, N., Liang, Z., 2025. Study on artificial neural networks and structure–activity relationship for constructing viscosity correlations of amine aqueous solutions based on chemical structure information. Sep Purif Technol 362, 131912. https://doi.org/10.1016/j.seppur.2025.131912.

Teng, Q., Wang, M., Niu, H., Cao, Y., Meng, Q., Jin, H., Jia, N., 2024. In-situ polymerized polyethyleneimine on porous polystyrene resin for highly efficient adsorption of CO2. J. Environ. Chem. Eng. 12 (5), 113652. https://doi.org/10.1016/j.jece.2024.113652.

Turgman-Cohen, S., Giannelis, E.P., Escobedo, F.A., 2015. Transport properties of amine/carbon dioxide reactive mixtures and implications to carbon Capture technologies. ACS Appl Mater Interfaces 7 (32), 17603–17613. https://doi.org/10.1021/acsami.5b04153.

Vallace, A., Ren, Y., Jones, C.W., Lively, R.P., 2023. Kinetic model describing self-limiting CO2 diffusion in supported amine adsorbents. Chem. Eng. J. 472, 144838. https://doi.org/10.1016/j.cej.2023.144838.

Vanini, M., Khodayari, A., Eyck, D.v., Seveno, D., 2023. Molecular dynamics simulations of the interactions between CO2 and branched unreacted and reacted polyethylenimine films. Gas Sci. Eng. 111, 204928. https://doi.org/10.1016/j.jgsce.2023.204928.

Veluturla, S., Singh, S., Fatima, S., 2025. A comprehensive review of carbon dioxide sequestration: exploring diverse methods for effective post combustion CO2 capture, transport, and storage. Environ. Eng. Res. 30 (1). https://doi.org/10.4491/eer.2023.452, 230452-230450.

Wang, D., Wang, X., Ma, X., Fillerup, E., Song, C., 2014. Three-dimensional molecular basket sorbents for CO2 capture: effects of pore structure of supports and loading level of polyethylenimine. Catal Today 233, 100–107. https://doi.org/10.1016/j.cattod.2014.01.038.

Wang, H., 2021. Model and experimental research on gas-solid reaction kinetics in thermochemical heat storage. Tsinghua University.

Wang, S., Li, Y., Li, Z., 2020. Fast adsorption kinetics of CO2 on solid amine sorbent measured using microfluidized bed thermogravimetric analysis. Ind Eng Chem Res 59 (15), 6855–6866. https://doi.org/10.1021/acs.iecr.9b05386.

Wang, S., Wang, S., Zhuo, Y., 2025. Rapid post-combustion CO2 capture by thermostatic concentration swing adsorption for amine-functionalized Al2O3. Fuel 402, 136003. https://doi.org/10.1016/j.fuel.2025.136003.

Wang, T., Liu, J., Huang, H., Fang, M., Luo, Z., 2016. Preparation and kinetics of a heterogeneous sorbent for CO2 capture from the atmosphere. Chem. Eng. J. 284, 679–686. https://doi.org/10.1016/j.cej.2015.09.009.

Wang, X., Ma, X., Song, C., Locke, D.R., Siefert, S., Winans, R.E., Möllmer, J., Lange, M., Möller, A., Gläser, R., 2013. Molecular basket sorbents polyethylenimine–SBA-15 for CO2 capture from flue gas: characterization and sorption properties. Microporous Mesoporous Mater. 169, 103–111. https://doi.org/10.1016/j.micromeso.2012.09.023.

Wilczak, A., Keinath, T.M., 1993. Kinetics of sorption and desorption of copper(II) and lead (II) on activated carbon. Water Environ. Res. 65 (3), 238–244. https://doi.org/10.2175/WER.65.3.7.

Xu, S., Huang, J., Wei, X., Chen, Y., Liu, M., Wu, J., Liu, Y., 2024. Preparation of amine functionalized micro-mesoporous silicon adsorbent from fly ash and its kinetic characteristics of CO2 adsorption/desorption process. Ceram Int 50 (14), 25150–25160. https://doi.org/10.1016/j.ceramint.2024.04.244.

Yan, H., Zhang, G., Liu, J., Li, G., Zhao, Y., Wang, Y., Wu, C., Wu, W., 2023. Amine-functionalized disordered hierarchical porous silica derived from blast furnace slag with high adsorption capability and cyclic stability for CO2 adsorption. Chem. Eng. J. 478, 147480. https://doi.org/10.1016/j.cej.2023.147480.

Yang, F., Zhu, X., Wu, J., Wang, R., Ge, T., 2022. Kinetics and mechanism analysis of CO2 adsorption on LiX@ZIF-8 with core shell structure. Powder Technol 399, 117090. https://doi.org/10.1016/j.powtec.2021.117090.

Yang, M., Wang, S., Xu, L., 2023. Hydrophobic functionalized amine-impregnated resin for CO2 capture in humid air. Sep Purif Technol 315, 123606. https://doi.org/10.1016/j.seppur.2023.123606.

Yang, X., Li, Z., Wang, Y., Song, Q., 2024. Influence of flue gas components on SO2 adsorption by activated carbon at low temperature. Chem. Eng. J. 499, 156265. https://doi.org/10.1016/j.cej.2024.156265.

Younas, M., Rezakazemi, M., Daud, M., Wazir, M.B., Ahmad, S., Ullah, N., Inamuddin, Ramakrishna, S., 2020. Recent progress and remaining challenges in post-combustion CO2 capture using metal-organic frameworks (MOFs). Prog Energy Combust Sci 80, 100849. https://doi.org/10.1016/j.pecs.2020.100849.

Zang, P., Tang, J., Zhang, H., Wang, X., Cui, L., Chen, J., Zhao, P., Dong, Y., 2024. Two-dimensional interfacial enhanced CO2 adsorption performance of porous organic amine solids: structure-activity relationships and DFT calculations. Chem. Eng. J. 485, 149938. https://doi.org/10.1016/j.cej.2024.149938.

Zhang, H., Goeppert, A., Czaun, M., Prakash, G.K.S., Olah, G.A., 2014. CO2 capture on easily regenerable hybrid adsorbents based on polyamines and mesocellular silica foam. Effect of pore volume of the support and polyamine molecular weight. RSC Adv 4 (37), 19403–19417. https://doi.org/10.1039/C4RA02145B.

Zhang, P., Ding, X., Ji, Y., Wang, R., Xie, J., Zhao, K., Fu, D., Wang, L., 2024. CO2 capture performance, kinetic and corrosion characteristics study of CO2 capture by blended amine aqueous solutions based on 1-(2-hydroxyethyl) piperidine. Int. J. Greenh. Gas Control 137, 104218. https://doi.org/10.1016/j.ijggc.2024.104218.

Zhang, R., Wang, X., Liu, S., He, L., Song, C., Jiang, X., Blach, T.P., 2019. Discovering inherent characteristics of polyethylenimine-functionalized porous materials for CO2 capture. ACS Appl Mater Interfaces 11 (40), 36515–36524. https://doi.org/10.1021/acsami.9b08496.

Zhao, P., Zhang, G., Yan, H., Zhao, Y., 2021. The latest development on amine functionalized solid adsorbents for post-combustion CO2 capture: analysis review. Chin. J. Chem. Eng 35, 17–43. https://doi.org/10.1016/j.cjche.2020.11.028.